Title

A Chemical Approach for Profiling Intracellular AKT Signaling Dynamics from Single Cells

Journal

Journal of the American Chemical Society, 140(42)

ISSN

0002-7863

Authors

Shao, Shiqun
Li, Zhonghan
Cheng, Hanjun
et al.

Publication Date

2018-10-24

DOI

10.1021/jacs.8b08931

Peer reviewed

HHS Public Access

Author manuscript

J Am Chem Soc. Author manuscript; available in PMC 2019 October 24.

Published in final edited form as:

J Am Chem Soc. 2018 October 24; 140(42): 13586–13589. doi:10.1021/jacs.8b08931.

A Chemical Approach for Profiling Intracellular AKT Signaling Dynamics from Single Cells

Shiqun Shao[†], **Zhonghan Li**[†], **Hanjun Cheng**[‡], **Siwen Wang**[†], **Nicole G. Perkins**[†], **Priyanka Sarkar**[†], **Wei Wei**[‡], and **Min Xue**[†]

[†]Department of Chemistry, University of California, Riverside, Riverside, California 92521, United States

[‡]Institute for Systems Biology, Seattle, Washington 98109, United States

Abstract

We present here a novel chemical method to continuously analyze intracellular AKT signaling activities at single-cell resolution, without genetic manipulations. A pair of cyclic peptide-based fluorescent probes were developed to recognize the phosphorylated Ser474 site and a distal epitope on AKT. A Förster resonance energy transfer signal is generated upon concurrent binding of the two probes onto the same AKT protein, which is contingent upon the Ser474 phosphorylation. Intracellular delivery of the probes enabled dynamic measurements of the AKT signaling activities. We further implemented this detection strategy on a microwell single-cell platform, and interrogated the AKT signaling dynamics in a human glioblastoma cell line. We resolved unique features of the single-cell signaling dynamics following different perturbations. Our study provided the first example of monitoring the temporal evolution of cellular signaling heterogeneities and unveiled biological information that was inaccessible to other methods.

Increasing evidence has demonstrated that the signaling activities in many biological systems are highly heterogeneous, as exemplified by cancer. The prominent inter- and intra-tumoral heterogeneities confer selection advantages that facilitate tumor progression, and contribute to drug resistance.[1–3] Recent advances in single-cell analytical methods have resolved such heterogeneities in many model systems and in patient samples. They have provided a clarifying and functional view on cellular heterogeneity, and its associated therapeutic implications.[4–7]

Nevertheless, single-cell studies can be confounded by the dynamic nature of the protein signaling processes. Conventional approaches for studying intracellular signaling activities, such as mass spectrometry and immuno-labeling, are destructive and not suitable for continuously analyzing living cells.[8–12] Consequently, single-cell implementations of those methods can only provide snapshot measurements.[7] A common strategy that overcomes such restriction is to employ genetically-encoded reporters.[13,14] However, such

Corresponding Author: min.xue@ucr.edu.

Supporting Information

Development, synthesis and characterization of the probes, validation of the binding affinities, cell culture, microscopy methods, data analyses and other experimental details. This information is available free of charge on the ACS Publications website.

manipulations may lead to strong interferences of the protein functions. Also, genetic modifications require complicated and laborious procedures, and cannot be readily employed to analyze clinical samples. Therefore, those methods provide limited translational value.

Herein, we report on the continuous interrogation of intracellular AKT signaling activities in single cells, using epitope-targeting fluorescent probes. For proof of concept, we chose AKT as a target protein to monitor its signaling dynamics. AKT plays a crucial role in cell survival, and is highly involved in the process of oncogenesis and tumor maintenance in many cancers.[15] Its activity is dependent on the phosphorylation status of several serine/tyrosine residues. Here we focused on the Ser473/474/472 site, which is the checkpoint for the full kinase capacity and is conserved among all three AKT isoforms.[15] We use the canonical sequence of AKT2 to represent those of the three isoforms.

We employed a Förster resonance energy transfer (FRET) strategy to probe the phospho-Ser474 (p-Ser474) status (Figure 1a). A cyclic peptide (cy-GSQTH) recognizing the K386-S398 epitope on AKT2 was developed through library screening processes (Figure S1–S4), and was labeled with a Rhodamine-B tag (probe **1**; Figure 1b and S5). Meanwhile, a previously reported sequence (cy-YYTYT), which was specific for the p-Ser474 site, was conjugated with a Cy5 moiety (probe 2; Figure 1b and S6).[16] Simultaneous binding of these two probes onto the same AKT protein generates FRET signals, which is contingent upon the phosphorylation of the Ser474 site. A dynamic reporting system can thus be realized.

The binding affinity of probe **1** towards the K386-S398 epitope (Figure S7 and S8) was validated using various strategies. Consistent results were obtained, demonstrating Kd values in the low nM range (Figure S9). Further validations using full-length recombinant AKT proteins yielded Kd values of 4.38 nM for AKT1 and 1.54 nM for AKT2 (Figure S10a). The binding affinity of probe **1** to full-length AKT3 was weaker (Kd = 19 nM, Figure S10b), which was probably due to its slight variation of the epitope sequence. Similarly, the Kd between probe **2** and the p-Ser474 epitope was determined to be in the high nM range, and it was sensitive to the phosphorylation status (Figure S11–S13).

We tested the function of the FRET reporting system using U87 cell lysates. U87 is a human glioblastoma cell line, where the EGFR-PI3K-AKT signaling pathways are essential to the metabolic maintenance and cell survival.[17,18] As shown in Figure 1c and S14, lysates from epidermal growth factor (EGF)-simulated cells exhibited an elevated FRET efficiency, comparing to that from control cells. This enhanced signal was significantly dampened following the treatment of AZD8055, an mTORC1/C2 inhibitor.[17,19] These results were consistent with the immunoblot result (Figure 1d), as well as the well-known structure of the EGFR-AKT signaling axes and the mechanisms of the Ser474 phosphorylation.[19]

The two probes must reside in the cytoplasm to interrogate the AKT signaling in living cells. We found that probe **1** was membrane impermeable (Figure S15). However, probe **2** could pass the cell membrane and accumulate inside the cells, pointing to an unknown transportation mechanism (Figure S16). In order to introduce both probes to the cytosol with a consistent ratio, we employed a well-established fusogenic liposomal formulation to

perform intracellular delivery (Figure 2a).[20] We followed standard protocols to prepare the liposomes and validated their cytosolic delivery capabilities (Figure S17 and S18). The delivery system led to the accumulation of probes inside cells (Figure S19). We also proved that these liposomes were nontoxic across a wide range of concentrations (Figure S20).

We then implemented the FRET system on a microchip platform to achieve single-cell resolution (Figure 2b).[21,22] The chip contains 57,600 addressable micro-wells, each with a diameter of 30 μm. These wells could trap the cells to allow precise tracking of individual cells. To load the cells onto the chip, a single-cell suspension (200k cells/mL) was placed on the chip and incubated for 30 min. During this time, cells randomly sank into the wells. The excess cells outside of the wells were scraped off gently, and fresh medium was applied to cover the chip. Selected areas containing 289 micro-wells were continuously imaged by a confocal microscope under cell culture conditions. The pinhole was kept wide open to cover the majority of the cells on the z-direction. Fluorescence intensities from the FRET channel were extracted and the inter-channel crosstalk was corrected to calculate the FRET signal for each single cell. In order to compensate the photo-bleaching effect and the cellular variances in the delivered probe concentrations, the apparent FRET signal was recalibrated using the Cy5 channel intensity (Figure S21). The results from different image frames were compiled to generate single-cell trajectories of the AKT signaling activities (Figure 2c).

We first evaluated the AKT signaling dynamics under basal conditions. As expected, the average signaling level remained unchanged throughout the course (Figure 2c). The distribution of signaling activities at the single-cell level had no time-dependent features. (Figure 2d and S22). However, a closer examination revealed prominent signaling fluctuations in many single cells. Consequently, the signaling variances among cells were highly time-dependent and incoherent (Figure S23). These results revealed that while snap-shot measurements can capture the sample distribution, the intensity-based identification of outliers can lead to invalid conclusions.

To further validate our method, we performed three sets of experiments involving different perturbations. In the first test, cells were treated with serum-free medium. We observed decreasing AKT activities in all single cells, which leveled off after 50 minutes (Figure 3a and S24). The temporal profile of the average signal was consistent with the immunoblot results (Figure 3b and S24d). Additionally, we found that the response rates varied significantly across the single cells, indicating differential efficiencies in the EGFR-PI3K-AKT signaling relay processes (Figure 3c).

In another experiment, the cells were treated with serum-free medium for one hour, followed by a one-hour EGF stimulation. Images were continuously taken throughout the course. Afterwards, the cells were fixed and permeabilized to remove the probes (Figure S25), and the cellular EGFR expression levels were determined by immunofluorescence (Figure 4a). As expected, serum starvation caused decreasing AKT signaling activities, and EGF stimulation led to a rapid recovery (Figure 4b). The response profile of the ensemble average was again consistent with the immunoblot results (Figure 4c).

We then sought to demonstrate that the time-resolved single-cell dataset provides rich and unique information that was inaccessible to other approaches. We extracted four orthogonal parameters from each single-cell trajectory: the decreasing rate before EGF-stimulation, the initial response rate after EGF-stimulation, the maximum increasing rate after EGF-stimulation, and the average signal intensity (Figure S26). We combined these four parameters with the EGFR expression level and constructed a new single-cell dataset for multivariate analyses. We observed three distinct subpopulations from the 186 single cells (Figure 4d). Notably, cells from one cluster exhibited significantly higher EGFR expression levels, comparing to other cells. Further analyses revealed that such features also accompanied higher signaling response rates upon EGF stimulation (Figure 4e). However, no individual cluster exhibited significant correlation between the response rate and the EGFR level (Figure S27). These results indicated that the heterogeneity in the EGFR-AKT signal relaying efficiencies were not exclusively dependent on the EGFR expression levels.

As a final validation experiment, we treated the cells with erlotinib, an FDA-approved EGFR inhibitor, and interrogated the single-cell signaling dynamics responses (Figure 4a). U87 cells are PTEN-deficient, therefore the EGFR inhibition could not properly translate to decreased AKT signaling activities.[23] As shown in Figure 4f, no noticeable trend was present in the average AKT signaling levels. This result was consistent with the immunoblot results (Figure 4g). However, both the magnitude and the frequency of the average signaling level fluctuation increased upon erlotinib-treatment (Figure 4f), demonstrating that erlotinib posed a strong perturbation to the signaling dynamics.

In order to resolve the effect of the erlotinib perturbation at the single-cell level, we examined the histograms of AKT signaling activities at each time point. However, no apparent subpopulations were observed (Figure S28). We then examined the autocorrelation signatures in the trajectories. We found that erlotinib treatment increased the number of cells whose signaling trajectories were autocorrelated (Figure S29). In other words, the AKT signaling fluctuations in these cells became slower, so that they could be resolved at our sampling rate (5 minutes). More interestingly, the autocorrelated cells exhibited a significantly higher EGFR expression level (Figure 4h and 4i). These observations open up biological questions that shall be the subject of other studies, but also point to the value of our measurements for uncovering new biology.

In conclusion, we have demonstrated the single-cell profiling of AKT signaling dynamics, using fluorescently-labeled epitope-targeting peptide probes and a micro-well chip platform. This reported method enables access to a new dimension of biological information. Multiplexing such detection schemes may permit a new field of study – single-cell dynamicomics, where the signaling dynamics of many pathways are simultaneously analyzed. In addition, we envision that this platform can be integrated with other micro-chip-based single-cell technologies, such as the single-cell proteomic and transcriptomic platforms, to achieve time-resolved multi-omics measurements.[24]

Supplementary Material

Refer to Web version on PubMed Central for supplementary material.

ACKNOWLEDGMENT

We gratefully acknowledge NIH U54 CA199090, U01 CA217655 and the Phelps Family Foundation for financial support. We thank Prof. David Nathanson and Dr. JingXin Liang for valuable discussions.

REFERENCES

(1). Lim JS; Ibaseta A; Fischer MM; Cancilla B; O'Young G; Cristea S; Luca VC; Yang D; Jahchan NS; Hamard C; Antoine M; Wislez M; Kong C; Cain J; Liu YW; Kapoun AM; Garcia KC; Hoey T; Murriel CL; Sage J Nature 2017, 545, 360. [PubMed: 28489825]

(2). McGranahan N; Swanton C Cell 2017, 168, 613. [PubMed: 28187284]

(3). Welch DR Cancer Res 2016, 76, 4. [PubMed: 26729788]

(4). Gawad C; Koh W; Quake SR Nat. Rev. Genet 2016, 17, 175. [PubMed: 26806412]

(5). Prakadan SM; Shalek AK; Weitz DA Nat. Rev. Genet 2017, 18, 345. [PubMed: 28392571]

(6). Spitzer Matthew H.; Nolan Garry P. Cell 2016, 165, 780. [PubMed: 27153492]

(7). Yu J; Zhou J; Sutherland A; Wei W; Shin YS; Xue M; Heath JR Annu. Rev. Anal. Chem 2014, 7, 275.

(8). Ong SE; Mann M Nat. Chem. Biol 2005, 1, 252. [PubMed: 16408053]

(9). Altelaar AF; Munoz J; Heck AJ Nat. Rev. Genet 2013, 14, 35. [PubMed: 23207911]

(10). Cox J; Mann M Nat. Biotechnol 2008, 26, 1367. [PubMed: 19029910]

(11). Larance M; Lamond AI Nat. Rev. Mol. Cell Biol 2015, 16, 269. [PubMed: 25857810]

(12). Haab BB Proteomics 2003, 3, 2116. [PubMed: 14595810]

(13). Miyawaki A Dev.Cell 2003, 4, 295. [PubMed: 12636912]

(14). Verveer PJ; Wouters FS; Reynolds AR; Bastiaens PIH Science 2000, 290, 1567. [PubMed: 11090353]

(15). Manning BD; Toker A Cell 2017, 169, 381. [PubMed: 28431241]

(16). Das S; Nag A; Liang J; Bunck DN; Umeda A; Farrow B; Coppock MB; Sarkes DA; Finch AS; Agnew HD; Pitram S; Lai B; Yu MB; Museth AK; Deyle KM; Lepe B; Rodriguez-Rivera FP; McCarthy A; Alvarez-Villalonga B; Chen A; Heath J; Stratis-Cullum DN; Heath JR Angew. Chem. Int. Ed. Engl 2015, 54, 13219. [PubMed: 26377818]

(17). Fan Q-W; Weiss WA Curr. Top. Microbiol. Immunol 2010, 347, 279. [PubMed: 20535652]

(18). Langhans J; Schneele L; Trenkler N; von Bandemer H; Nonnenmacher L; Karpel-Massler G; Siegelin MD; Zhou S; Halatsch M-E; Debatin K-M; Westhoff M-A Oncogenesis 2017, 6, 398. [PubMed: 29184057]

(19). Chresta CM; Davies BR; Hickson I; Harding T; Cosulich S; Critchlow SE; Vincent JP; Ellston R; Jones D; Sini P; James D; Howard Z; Dudley P; Hughes G; Smith L; Maguire S; Hummersone M; Malagu K; Menear K; Jenkins R; Jacobsen M; Smith GCM; Guichard S; Pass M Cancer Res 2010, 7, 288.

(20). Kube S; Hersch N; Naumovska E; Gensch T; Hendriks J; Franzen A; Landvogt L; Siebrasse JP; Kubitscheck U; Hoffmann B; Merkel R; Csiszar A Langmuir 2017, 33, 1051. [PubMed: 28059515]

(21). Rettig JR; Folch A Anal. Chem 2005, 77, 5628. [PubMed: 16131075]

(22). Tang Y; Wang Z; Li Z; Kim J; Deng Y; Li Y; Heath JR; Wei W; Lu S; Shi Q Proc. Natl. Acad. Sci. U.S.A 2017, 114, 2544. [PubMed: 28223509]

(23). Wang MY; Lu KV; Zhu S; Dia EQ; Vivanco I; Shackleford GM; Cavenee WK; Mellinghoff IK; Cloughesy TF; Sawyers CL; Mischel PS Cancer Res 2006, 66, 7864. [PubMed: 16912159]

(24). Heath JR; Ribas A; Mischel PS Nat. Rev. Drug Disc 2015, 15, 204.

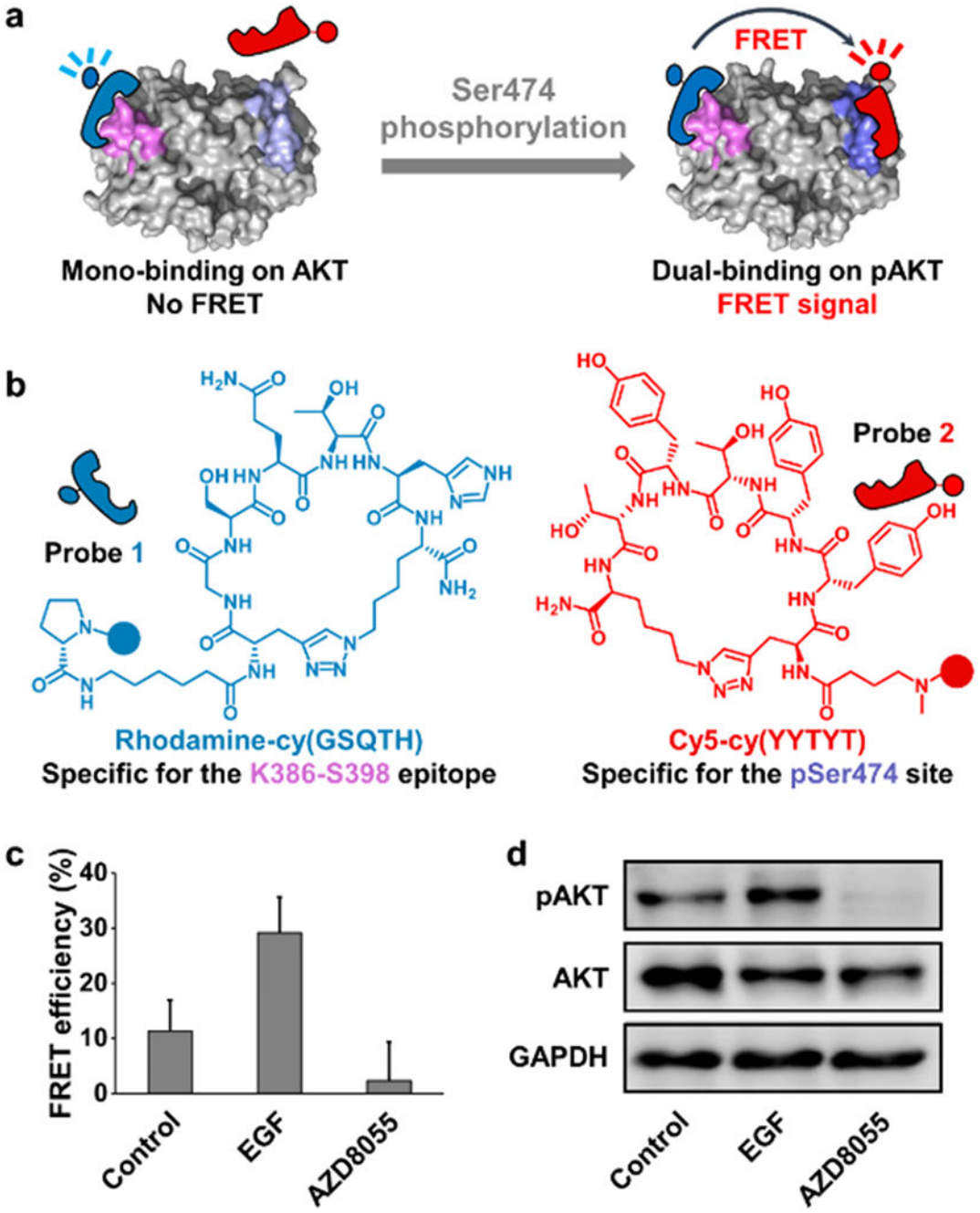

Figure 1.

(a) The FRET-based pAKT detection method. **(b)** Structures of probe **1** and probe **2**. **(c-d)** Serum-starved U87 cells were sequentially treated with EGF (50 ng/mL in full medium, 15 min) and AZD8055 (1 μM in full medium, 30 min). Cell lysates were obtained at each stage. **(c)** FRET efficiency between probe 1 (200 nM) and probe 2 (50 nM) when incubated with the cell lysates (10 μg protein content). Seven replicates were conducted. **(d)** Validation of the pAKT levels in the cell lysates.

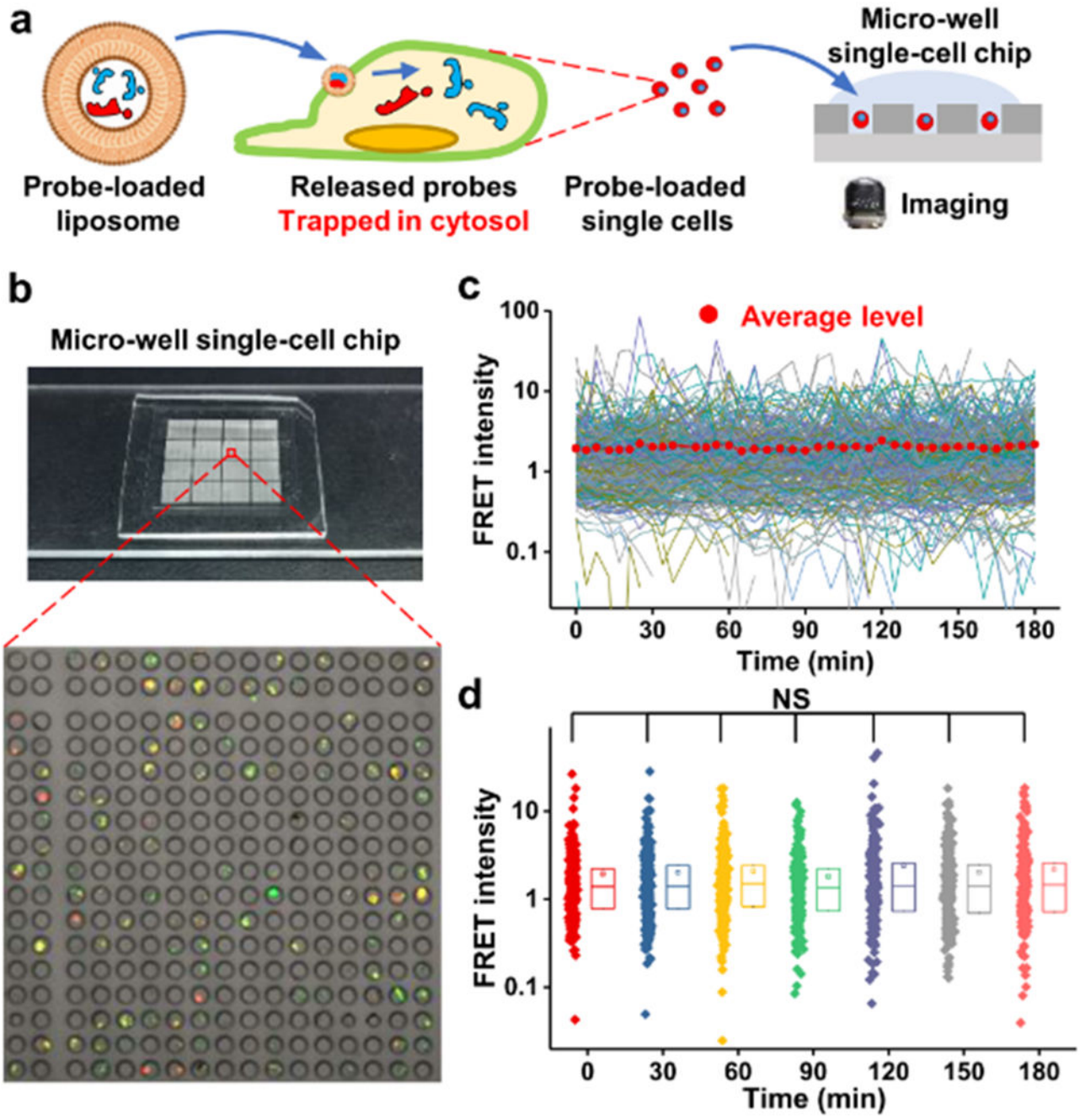

Figure 2.

(a) Cytosolic delivery of the probes using liposomes enables dynamic interrogation of the AKT signaling. The micro-well chip provides single-cell data resolution. **(b)** The picture of the micro-well chip and a representative confocal image. **(c)** Basal single-cell trajectories of the AKT signaling dynamics from 270 U87 cells cultured in full medium. **(d)** Snapshot-type single-cell datasets extracted from the time-resolved trajectories. NS, No significant difference.

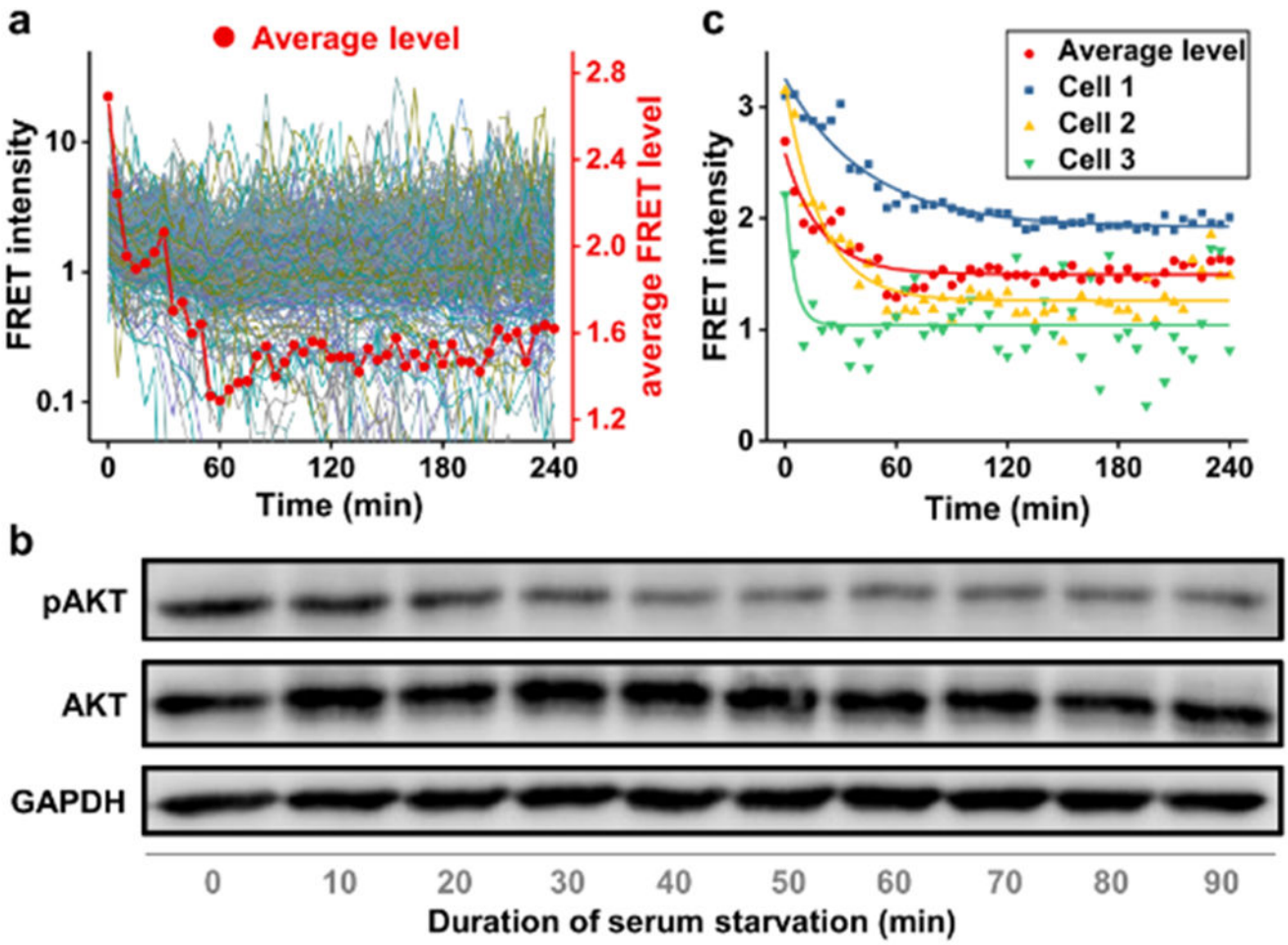

Figure 3.

(a) Single-cell AKT signaling trajectories from 280 serum-starved U87 cells. **(b)** Immunoblot analyses of the pAKT levels in serum-starved U87 cells. **(c)** Selected single-cell trajectories demonstrating the differential response rates among cells.

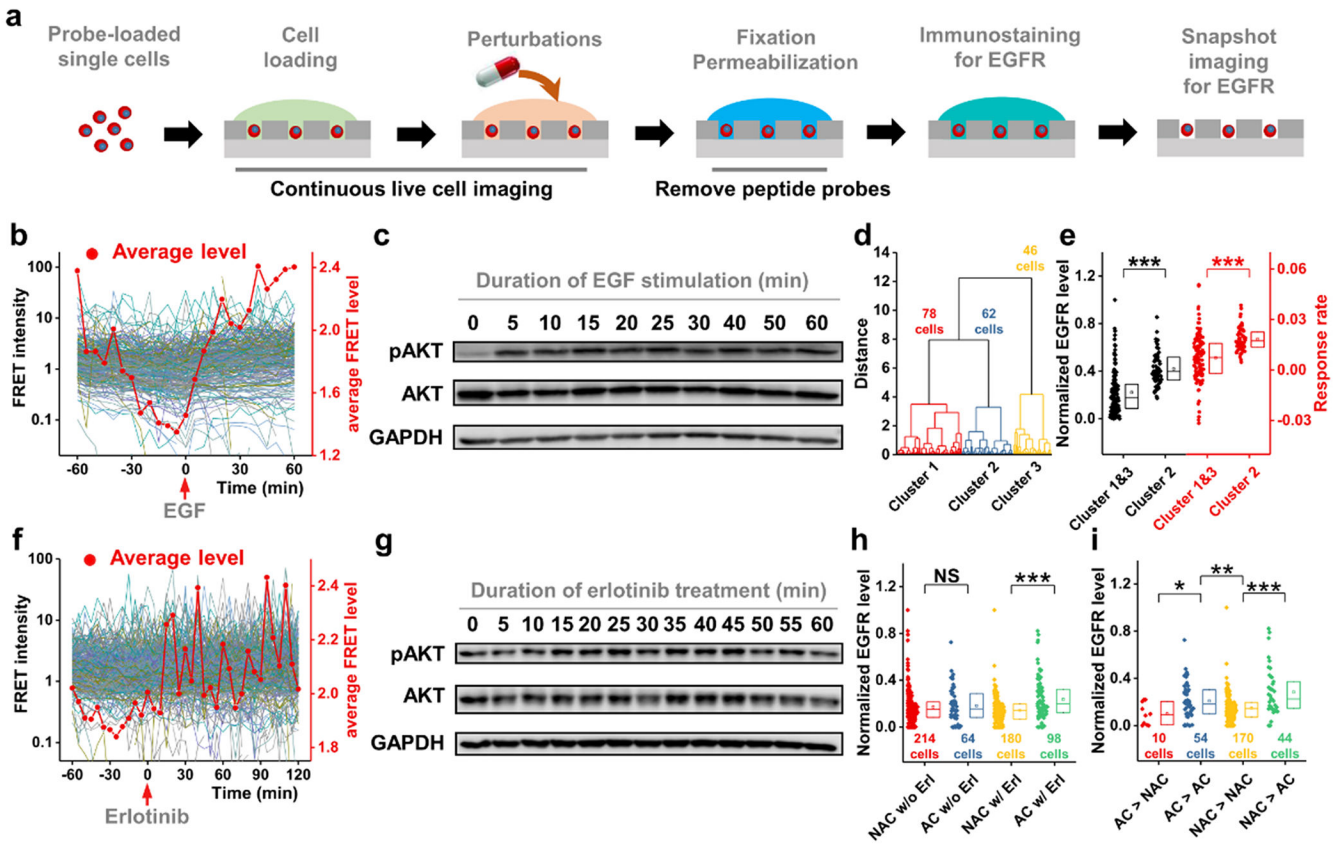

Figure 4.

Detection of AKT signaling dynamics in U87 cells exposed to different perturbations. **(a)** The workflow of the experiments. **(b)** Single-cell AKT signaling trajectories in response to serum starvation and EGF stimulation (50 ng/mL in full medium). **(c)** pAKT levels in response to EGF stimulation detected at bulk level. **(d)** Hierarchical clustering of the processed single-cell dataset. **(e)** Comparison of the EGFR levels and the EGF-induced response rates between Cluster 2 and Cluster 1&3. **(f)** Single-cell AKT signaling trajectories in response to 10 μM erlotinib treatment. Cells were cultured in full media throughout this experiment. **(g)** pAKT levels in response to erlotinib treatment detected at bulk level. **(h)** The EGFR expression levels in non-autocorrelated cells and autocorrelated cells populated before and after the erlotinib-treatment. **(i)** The EGFR expression levels in cells that were separated from their original groups by erlotinib treatment. NS, no significant difference; *p < 0.05; **p < 0.01; ***p < 0.001. Erl, erlotinib; NAC, non-autocorrelated; AC, autocorrelated.